Available online at www.sciencedirect.com

ScienceDirect

Mendeleev Commun., 2023, **33**, 349–352

Mendeleev Communications

Titanium dioxide nanoparticles heavily doped with niobium: a light-induced electron paramagnetic resonance study

Vladimir Yu. Osipov,*[a,b†] Dong Hao,[c,d†] Kazuyuki Takai,[b] Tetsuo Uchikoshi,[c,e] Hironori Ogata[b,c] and Takamasa Ishigaki[b,c]

[a] *Ioffe Institute, 194021 St. Petersburg, Russian Federation. E-mail: osipov@mail.ioffe.ru*
[b] *Department of Chemical Science and Technology, Faculty of Bioscience and Applied Chemistry, Hosei University, Koganei, Tokyo 184-8584, Japan*
[c] *Research Center for Micro-Nano Technology, Hosei University, Koganei, Tokyo 184-0003, Japan*
[d] *Ceramic Research Center, Saga University, Arita, Saga 844-0013, Japan*
[e] *Research Center for Functional Materials, National Institute for Material Science, Tsukuba, Ibaraki 305-0047, Japan*

DOI: 10.1016/j.mencom.2023.04.017

Light-induced electron paramagnetic resonance (EPR) spectra of titanium dioxide nanoparticles heavily doped with niobium(V) are studied. At low temperatures, the EPR signal caused by interband illumination is associated with paramagnetic Ti^{3+} sites in anatase, which, as the temperature rises above 210 K, are discharged to the non-paramagnetic Ti^{4+} state due to the escape of trapped photoelectrons and their recombination with holes. The temperature dependence of the integral EPR signal has a non-Curie character, especially in the temperature range where the discharge of Ti^{3+} centers is already significant.

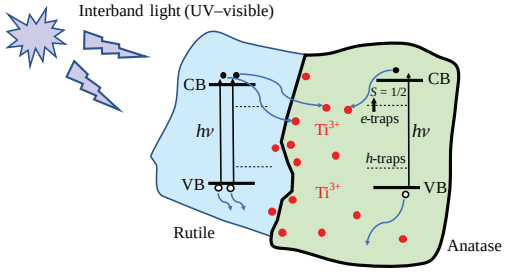

Scheme of interband optical transitions leading to the capture of photoelectrons in rutile–anatase compound particles.

Keywords: titanium dioxide, niobium, photocatalysts, electron paramagnetic resonance, electron and hole traps, charge transfer.

Topical modern trends in magnetochemistry involve studies by the method of electron paramagnetic resonance (EPR) of new crystalline catalysts, electrode materials for electrochemistry and carriers of new catalytically active agents at the atomic level.[1,2] One such material is titanium dioxide.[3] Conventional TiO_2 for photocatalysis is a pure anatase phase,[4] which transforms into a rutile phase upon annealing above ~700 °C.[5,6] The anatase phase has excellent photocatalytic activity when irradiated with UV light. Degussa P25 is a conventional custom-synthesized commercial mixed-phase nanoscale TiO_2 powder that contains ~80% of anatase phase and ~20% of rutile phase.[7] In a photocatalytic field, it is seen as the most effective photocatalyst and can be used to purify water from many harmful contaminants.[7–11] A certain photocatalytic activity is obtained even under the visible light irradiation. Enhanced photocatalytic properties of the mixed phase material arise from the fact that when irradiated with UV–visible light (photon energies above 3.0 eV), photogenerated charge carriers are effectively separated.[12,13] Electrons photogenerated in rutile (direct band gap 3.0 eV) are transferred to anatase (band gap 3.2 eV) and are captured there by traps‡ located in the crystal lattice near the rutile–anatase heterointerface, while photoholes remaining in the rutile valence band are captured by surface or bulk hole traps in the rutile nanoparticles. The separation of charge carriers (e^-–h^+) contributes to the effectiveness of the photocatalytic properties of the material.

Nevertheless, further studies on increasing the photocatalytic activity of titanium dioxide nanoparticles in the form of anatase and rutile are extremely important. In this case, use is made of a variety of technological solutions such as, for example, the placement of TiO_2 nanoparticles on conductive graphene or reduced graphene oxide substrates and the use of nanostructured TiO_2 in the form of an array of nanotubes with a high aspect ratio.[14,15] All these methods are connected in one way or another with suppressing the recombination of photogenerated electron–hole pairs inside nanoparticles and ensuring the diffusion drift of carriers of the same type to the surface.

A stronger increase in photocatalytic properties, especially in visible light photocatalytic activity (when using light from the spectral range above 400 nm), is achieved by doping the titanium dioxide lattice with a number of dopant ions giving the impurity level in the bandgap. A mixture of niobium heavy-doped rutile and anatase nanoparticles (in an amount of up to 25 at%)§ of the nonequilibrium chemical composition was realized.[16] The 25 at% of Nb also means the upper limit of Nb^{5+} solubility in the host TiO_2 matrix. It should be noted that although such a content of niobium in doped titanium oxide is high, its structure of the nonequilibrium composition is very different from that for the compound of the stoichiometric composition $TiNb_2O_7$. The

† These authors contributed equally to this work.
‡ Such trapping sites are located 0.8 eV lower than the conduction band edge of anatase.

§ Percentage here means the proportion of niobium (Nb^{5+} and/or Nb^{4+}) in the total amount of metal cations: Nb/(Ti + Nb). That is, this is the fraction of niobium atoms in the cationic metal sublattice, which consists of two types of cations. This ratio is achieved when the number of doping niobium atoms is three times less than the number of titanium atoms: Ti/Nb = 3.

dominant lattice defect in the Nb-doped TiO_2 is interstitial oxygen with a net charge of –1. Structural and electrochemical properties of various specially prepared nanosized TiO_2 powders heavily doped with niobium have already been described in the literature.[17]

Since titanium dioxide doped with high concentrations of niobium is a unique material with excellent photocatalytic properties,[16,18,19] it was advisable to find its other unique characteristics, allowing it to be easily recognized among other materials. Such a characteristic property can be the appearance of a photo-EPR signal as a result of illumination with interband light at a low temperature with a specific dependence of its amplitude on temperature.[20] The purpose of this work was to study the main parameters of the photo-EPR signal for TiO_2 heavily doped with niobium as a function of temperature. EPR studies were carried out not only to examine the specific characteristics of light-induced EPR signals associated with charge traps in the new material, but also to possibly confirm the presence of charge transfer between anatase (A) and rutile (R) phases in neighboring particles touching each other.[21] For this study, niobium-doped samples were selected, synthesized by the thermal plasma method and demonstrating the highest photocatalytic characteristics among all differenty synthesized samples of similar composition.

Titanium dioxide doped with 25 at% Nb was synthesized through radio frequency thermal plasma processing. Details of the experimental setup and synthesis process could be found elsewhere.[22,23] Typically, tetrabutyl titanate and niobium(V) ethoxide with the prescribed molar ratio of Nb/(Ti + Nb) = 0.25 were used as a titanium source and a niobium source, respectively. Ethanolamine [$HN(OC_2H_5)_2$] was used as an inhibitor to prevent hydrolysis. The particle size of the as-synthesized thermal plasma 25 at% Nb-doped TiO_2 was approximately 20–30 nm. The heat treatment process was carried out in a program-controlled muffle furnace in order to increase the photocatalytic ability of the material. In a typical process, the as-synthesized powder was heated at 850 °C for 3 h in the air with a ramping rate of 5 °C min^{-1} and a cooling rate of 2 °C min^{-1}, respectively. After such heat treatment at 850 °C, the particle size increased to 50 nm. The grain growth was effectively inhibited by the high concentration of niobium doping. Doping with Nb^{5+} also prevented the narrowing of the TiO_2 band gap and saved photocatalytic properties after heat treatment.[23] The obtained sample was marked as TP-NTO850. In methyl orange degradation tests, it shows the highest visible-light photocatalytic performance compared to any other heat-treated (at various temperatures) 25 at% Nb-doped TiO_2 samples (Section S1, Online Supplementary Materials) and was selected for EPR studies.

The phase composition of TP-NTO850 determined by the analysis of its X-ray diffraction pattern by the Rietveld method is presented in Table 1. The true atomic content of niobium is almost as prescribed, but slightly higher, namely Nb/Ti = 0.352 (instead of 0.333), as shown by elemental analysis data obtained by atomic emission spectroscopy. An analysis of the elemental composition data for all three phases found by X-ray diffraction shows that the following ratio Nb/Ti = 0.225 takes place for the cationic sublattice of anatase and rutile phases. During processing at a temperature of 850 °C, part of anatase is transformed into rutile, which is a gradual process. In general, the rutile particles grow easily with the duration of the heat treatment and are found to be larger in size than the remaining anatase particles. Rutile and anatase nanoparticles are in close contact with each other and may even have a common heterointerface, since the grains grow and agglomerate during heat treatment. As a result, charge transfer can easily occur between particles of rutile, anatase, and $TiNb_2O_7$ upon photoexcitation of carriers.

Table 1 The phase composition of TP-NTO850 by Rietveld analysis.

Sample	Nb-doped rutile (mass%)	Nb-doped anatase (mass%)	$TiNb_2O_7$ (mass%)
TP-NTO850	65.2	15.0	19.8

The EPR spectra were recorded in the temperature range 100–300 K at a microwave frequency of ~9.08 GHz using an X-band EPR spectrometer. The powder sample in an amount of about 20–25 mg was introduced into a standard quartz EPR tube. The tube was not specially pumped out and the air was not removed from it. The upper end of the tube was isolated from the outside atmosphere (to prevent air infiltration into the tube and oxygen sorption on the material at low temperatures) by sealing with a paraffin film. A 500 W xenon short arc lamp with a heat absorbing glass filter (HA30, bandwidth of 300–900 nm)[¶] was used to irradiate the sample by UV–visible light and cut the infrared light from the light source for avoiding sample heating. The characteristics of the lamp and the transmission spectrum of the filter are given in the Online Supplementary Materials in Figure S1. The EPR spectra (spectra of the first derivative of absorption) of the sample were recorded at a microwave power of 2 mW in a mode far from the saturation of the EPR signal. The recording interval was from 313 to 343 mT on the magnetic field scale. The positions of the EPR lines on the magnetic field scale and the corresponding *g*-factors were precisely determined using an external Mn^{2+}/MgO standard giving six well-resolved equidistantly separated lines of a hyperfine structure of almost the same intensity. To quantify the intensity of the integrated EPR signal from the observed Ti^{3+} centers, each spectrum recorded at a fixed temperature was subjected to double integration with background correction in the spectrum of the integrated EPR signal obtained after the first integration.[††]

The following EPR results are from the TP-NTO850 sample showing the highest visible-light photocatalytic performance. The EPR spectra of this sample were recorded at 100 K both under dark conditions (without preliminary irradiation) and after exposure to UV–visible light for a fixed time, respectively. Firstly, the EPR spectrum was measured in the dark at 100 K, *i.e.* prior to any optical irradiation. We have reliably found that the TP-NTO850 sample does not show any EPR signals in the dark. It means that there are no paramagnetic spin-half species (dangling bonds or paramagnetic centers) in this as-cooled sample in dark conditions. At the same time, it also means that no transfer of electrons between the A- and R-phases leading to the appearance of spin-half species in anatase phase occurs at 100 K in the dark. When the sample was irradiated with UV–visible radiation[‡‡] for ~15 min, an EPR signal consisting of at least two components appeared on the magnetic field scale in the range from 323 to 334 mT. Its low-field (at ~325.4 mT) and high-field (~330.4 mT) components correspond to the *g*-values of 1.991 and 1.961, which can be precisely ascribed to the $g_\perp$ and $g_\parallel$ components of a signal related with paramagnetic Ti^{3+} species (S = 1/2, electronic configuration [Ar] $3d^1$) in the anatase phase, in full accordance with the works by Harum *et al*., Ide *et al*., and a few done a long time ago.[26–29] When the same sample warmed up to room temperature once and then freshly cooled in the dark

¶ Manufacturers: Ushio Lighting Inc., Japan (lamp) and Hoya Corporation, Japan (optical filter).

†† A method for estimating the integrated EPR signal intensity for isolated metal ions has been described, for example, in refs. 24, 25.

‡‡ For such irradiation, the light of a xenon short arc lamp passed through a HA30 filter was used. Similar results can be obtained when using a combination of Hoya filters (HA30 and L42) that transmit only visible radiation ($\lambda \geqslant 410$ nm), but the intensity of the photo-EPR signal is lower in this case.

was again used to record the EPR spectra at 100 K, no EPR signals were observed in dark conditions without its exposing to UV–visible light. After exposure to UV–visible light for 15 min, an EPR signal similar to the previous one appears with two components (with the same *g*-factors: $g_\perp = 1.991$, $g_\parallel = 1.961$). This indicates that the photoinduced EPR signal of the sample is completely reversible and is repeatedly reproduced after thermal cycles of heating to 300 K and cooling to 100 K, followed by illumination. This is due to the fact that many photogenerated electrons and holes appear during irradiation, and a certain part of the electrons is captured in the anatase phase of the hybrid material, which leads to a fixed value of the EPR signal associated with half-spin Ti^{3+} sites. This result means the high efficiency of the charge separation of photogenerated carries and that the resulting charge transfer between anatase and rutile phases is quite noticeable under the influence of UV–visible irradiation, which ultimately confirms the improved visible-light photocatalytic activity.[26,27] What is more, the existence of a Ti^{3+} photo-EPR signal ($g_\perp = 1.991$, $g_\parallel = 1.961$) undoubtly confirmed that the charge transfer of photogenerated electrons happens from the conduction band of rutile[§§] to the trapping sites (*e*-traps) laying in the bandgap of anatase, which is different from the case where only rutile phase serves as a matrix with trapping sites for photogenerated electrons.[16,30,31] Here we consider that a lot of EPR-silent Ti^{4+} sites ($S = 0$, electronic configuration [Ar]) located in the anatase capture the photogenerated electrons and become the spin-half Ti^{3+} species for a long time (a couple dozen hours at least) at cryogenic temperature due to the very low probability of reverse discharging these traps at 100 K. The radiation of a xenon lamp after passing through the HA30 filter has a spectral range of 300–950 nm (photon energies from 4.13 to 1.31 eV) and excites electron–hole pairs not only in the rutile phase ($E_g = 3.0$ eV), but also in the wider-gap anatase phase ($E_g = 3.2$ eV). Thus, electron traps of the anatase phase can also capture photoelectrons generated by interband light with an energy above 3.2 eV directly in anatase particles. The Ti^{3+} paramagnetic centers in this case are predominantly located inside the anatase particles, and not only at the interface between the crystalline phases. The corresponding scheme of optical transitions that create photocarriers and the approximate arrangement of Ti^{3+} centers in the particles are shown in the Figure S3 (Online Supplementary Materials). Photoelectrons can apparently also be captured in the rutile phase in the Ti^{3+} states (shallow electronic states) lying below the bottom of the rutile conduction band. However, in our case, we did not observe Ti^{3+} EPR signals from the rutile phase. This is due to the fact that such electron trapping sites in rutile should have EPR signals with $g_\perp = 1.975$ and $g_\parallel = 1.940$,[26] but they are absent in our EPR spectra.

The spectra of the photoinduced EPR signal produced by illumination with interband light at 100 K are shown in Figure 1(*a*),(*b*) for different fixed temperatures in the range up to 200 K. It can be seen that with increasing temperature, the peak intensities of all EPR spectrum components decrease. In this case, the widths (ΔH_{pp})[¶¶] of the individual signal components, for example, the high-intensity component with a *g*-factor of 1.991, gradually increase with increasing temperature. An analysis of the temperature behavior of the integrated intensity[†††]

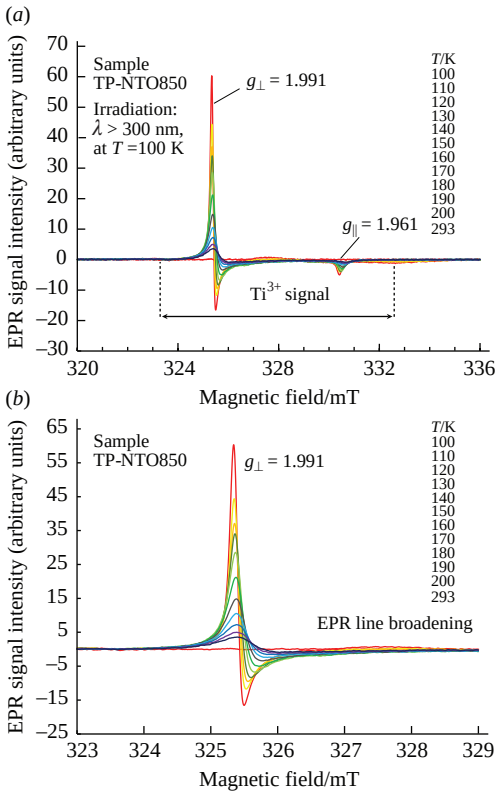

Figure 1 EPR spectra of a TP-NTO850 sample at different temperatures (after illumination by a xenon lamp at a temperature of 100 K for ~15 min): (*a*) in a wide range of the magnetic field and (*b*) in a narrow range around the line $g_\perp = 1.991$. The twelve spectra corresponding to different temperatures from 100 to 293 K are highlighted in color. The microwave frequency $\nu = 9.078$ GHz, and the microwave power $P_{MW} = 2$ mW.

of the EPR spectrum of the TP-NTO850 sample is shown in Figure 2. In this figure, circles are experimental points and the solid red line reflects the hypothetical behavior of the EPR spin susceptibility according to the Curie–Weiss law with a Weiss temperature of about ~40 K. It can be seen that the temperature dependence of the integrated intensity of the EPR signal is not of the Curie type, and at temperatures above 150 K, there is a rapid decrease in the signal intensity, probably due to the recharging of paramagnetic states according to the $Ti^{3+} \rightarrow Ti^{4+} + \bar{e}$ scheme and the escape of electrons from these sites. It is noteworthy that after the return cooling from 175 to 100 K (in the dark), the EPR signal is restored almost completely (by 95–97% in terms of the peak amplitude of the narrow low-field component with $g_\perp = 1.991$). This indicates that heating to ~175 K does not yet lead to a noticeable escape of trapped electrons from the Ti^{3+}

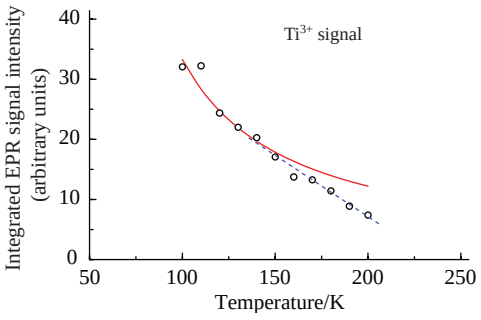

Figure 2 Temperature dependence of the intensity of the integrated photo-EPR signal associated with paramagnetic $S = 1/2$ Ti^{4+}/Ti^{3+} sites in anatase that have captured photoelectrons as a result of irradiation with interband light. Open circles are experimental points. The red line is the Curie curve plotted for spins with a Weiss temperature of +42 K, and the blue dashed curve illustrates the deviation from the Curie law at temperatures above 150 K.

[§§] Here we mean states above the bottom of the conduction band (CB) of rutile (see Figure S3 in Online Supplementary Materials).

[¶¶] Here we consider the peak-to-peak distance along the magnetic field scale as a linewidth.

[†††] An example of an integrated EPR absorption signal obtained by integrating the signal of the first derivative and corresponding to a temperature of 150 K is shown in Figure S2 (Online Supplementary Materials).

paramagnetic sites. The observed rapid (on the temperature scale) decrease in the EPR signal is apparently a characteristic feature of Ti^{3+} sites in the matrix of titanium dioxide polyforms doped with niobium.

Note that a similar temperature drop in the signal from Ti^{3+} sites with increasing temperature in the range up to 220 K was observed for anatase doped with niobium.[30] However, the temperature dependence of the integrated Ti^{3+} EPR signal was not investigated.[30] Also, in our case, no photo-EPR signal associated with the O^{-}* oxygen anion radical was found in the range of magnetic fields approximately 2–7 mT lower than the resonant field value for the EPR line with a *g*-factor of 1.991.

The non-Curie behavior of the photo-EPR signal associated with Ti^{3+} sites indicates a shallow occurrence of their energy levels compared to the edge of the conduction band of the corresponding phase of titanium dioxide and, possibly, the polaron character of such sites in the host matrix of Ti^{4+} sites. It is very interesting that the width of the EPR line with a *g*-factor of $g_{\perp} = 1.991$ increases relatively rapidly with increasing temperature. This indicates a possible delocalization of the Ti^{3+} spin, when a captured electron, which actually forms the spin of a particular Ti^{3+} site, is delocalized over a large number of neighboring Ti^{4+} sites of the crystal lattice and moves between them by means of hopping transfer.[30,32] In the temperature range 150–210 K, this delocalization becomes significant.

Polymorphic forms of titanium dioxide heavily doped with niobium exhibit an EPR signal from anatase Ti^{3+} sites[‡‡‡] as a result of illumination with interband light at cryogenic temperatures. The integral intensity of this signal decreases rapidly with increasing temperature according to the non-Curie law. At temperatures above 170–180 K, the processes associated with the thermalization of electrons from the Ti^{3+} levels into the conduction band of anatase and/or their recombination with holes released from shallow traps near the valence band of rutile come into force and the paramagnetic sites are discharged according to the scheme $Ti^{3+} \rightarrow Ti^{4+} + \bar{e}$. The EPR signal from Ti^{3+} sites irreversibly disappears upon heating to room temperature upon subsequent illumination with interband light at temperatures below 150 K.

V.O. thanks the Ioffe Institute for support (project 0040-2019-0013) and the Japan Society for the Promotion of Science for the JSPS Fellowship (L17526). K.T. acknowledges the support of JSPS KAKENHI (grant nos. 22K05056, 19K05410 and 26107532). D.H., H.O. and T.I. acknowledge the support of Grant-in-Aid of Building the Private University Strategic Research Base (S1311023) of the Ministry of Education, Culture, Sports, Science and Technology of Japan (MEXT, Japan).

Online Supplementary Materials

Supplementary data associated with this article can be found in the online version at doi: 10.1016/j.mencom.2023.04.017.

‡‡‡ These sites are mainly located at the anatase–rutile interface of tightly contacted nanoparticles.

References

1 M. Hunger and J. Weitkamp, *Angew. Chem., Int. Ed*., 2001, **40**, 2954.
2 S. Van Doorslaer and D. M. Murphy, in *EPR Spectroscopy. Topics in Current Chemistry*, eds. M. Drescher and G. Jeschke, Springer, Berlin, Hidelberg, 2011, vol. 321, pp. 1–39.
3 D. Chen and R. A. Caruso, *Adv. Funct. Mater.*, 2013, **23**, 1356.
4 J. Zhang, P. Zhou, J. Liu and J. Yu, *Phys. Chem. Chem. Phys*., 2014, **16**, 20382.
5 D. A. Hanaor and C. C. Sorrell, *J. Mater. Sci*., 2011, **46**, 855.
6 S.-C. Zhu, S.-H. Xie and Z.-P. Liu, *J. Am. Chem. Soc.*, 2015, **137**, 11532.
7 B. Ohtani, O. O. Prieto-Mahaney, D. Li and R. Abe, *J. Photochem. Photobiol., A*, 2010, **216**, 179.
8 H. Lu, B. Zhao, R. Pan, J. Yao, J. Qiu, L. Luo and Y. Liu, *RSC Adv*., 2014, **4**, 1128.
9 N. Bowering, G. S. Walker and P. G. Harrison, *Appl. Catal., B*, 2006, **62**, 208.
10 M. Janus and A. W. Morawski, *Appl. Catal., B*, 2007, **75**, 118.
11 A. Fujishima, T. N. Rao and D. A. Tryk, *J. Photochem. Photobiol., C*, 2000, **1**, 1.
12 T. Ishigaki, Y. Nakada, N. Tarutani, T. Uchikoshi, Y. Tsujimoto, M. Isobe, H. Ogata, C. Zhang and D. Hao, *R. Soc. Open Sci.*, 2020, **7**, 191539.
13 R. Su, R. Bechstein, L. Sø, R. T. Vang, M. Sillassen, B. Esbjörnsson, A. Palmqvist and F. Besenbacher, *J. Phys. Chem. C*, 2011, **115**, 24287.
14 Yu. V. Ioni, Yu. A. Groshkova, E. Yu. Buslaeva and S. P. Gubin, *Dokl. Chem.*, 2021, **501**, 255 (*Dokl. Ross. Akad. Nauk. Khim., Nauki Mater.*, 2021, **501**, 27).
15 A. A. Rempel, A. A. Valeeva, A. S. Vokhmintsev and I. A. Weinstein. *Russ. Chem. Rev.*, 2021, **90**, 1397.
16 N. Tarutani, R. Kato, T. Uchikoshi and T. Ishigaki, *Sci. Rep.*, 2021, **11**, 15236.
17 M. Lubke, J. Shin, P. Marchand, D. Brett, P. Shearing, Z. Liu and J. A. Darr, *J. Mater. Chem. A*, 2015, **3**, 22908.
18 M. Hirano and K. Matsushima. *J. Nanosci. Nanotechnol*., 2006, **6**, 762.
19 S. Khan, H. Cho, D. Kim, S. S. Han, K. H. Lee, S.-H. Cho, T. Song and H. Choi, *Appl. Catal., B*, 2017, **206**, 520.
20 J. Kiwi, J. T. Suss and S. Szapiro, *Chem. Phys. Lett.*, 1984, **106**, 135.
21 D. C. Hurum, A. G. Agrios, S. E. Crist, K. A. Gray, T. Rajh and M. C. Thurnauer, *J. Electron Spectrosc. Relat. Phenom.*, 2006, **150**, 155.
22 X. H. Wang, J.-G. Li, H. Kamiyama, M. Katada, N. Ohashi, Y. Moriyoshi and T. Ishigaki, *J. Am. Chem. Soc.*, 2005, **127**, 10982.
23 C. Zhang, M. Ikeda, T. Uchikoshi, J.-G. Li, T. Watanabe and T. Ishigaki, *J. Mater. Res.*, 2011, **26**, 658.
24 V. Yu. Osipov, F. M. Shakhov, N. M. Romanov and K. Takai, *Mendeleev Commun*., 2022, **32**, 645.
25 V. Yu. Osipov, N. M. Romanov, I. E. Suvorkova, E. V. Osipova, T. Tsuji, Y. Ishiguro and K. Takai, *Mendeleev Commun.*, 2022, **32**, 132.
26 D. C. Hurum, A. G. Agrios, K. A. Gray, T. Rajh and M. C. Thurnauer, *J. Phys. Chem. B*, 2003, **107**, 4545.
27 Y. Ide, N. Inami, H. Hattori, K. Saito, M. Sohmiya, N. Tsunoji, K. Komaguchi, T. Sano, Y. Bando, D. Golberg and Y. Sugahara, *Angew. Chem., Int. Ed*., 2016, **55**, 3600.
28 P. Meriaudeau, M. Che and C. K. Jørgensen, *Chem. Phys. Lett.*, 1970, **5**, 131.
29 O. I. Micic, Y. Zhang, K. R. Cromack, A. D. Trifunac and M. C. Thurnauer, *J. Phys. Chem*., 1993, **97**, 7277.
30 M. Chiesa, M. C. Paganini, S. Livraghi and E. Giamello, *Phys. Chem. Chem. Phys*., 2013, **15**, 9435.
31 D. O. Scanlon, C. W. Dunnill, J. Buckeridge, S. A. Shevlin, A. J. Logsdail, S. M. Woodley, C. R. A. Catlow, M. J. Powell, R. G. Palgrave, I. P. Parkin, G. W. Watson, T. W. Keal, P. Sherwood, A. Walsh and A. A. Sokol, *Nat. Mater.*, 2013, **12**, 798.
32 A. R. Elmaslmane, M. B. Watkins and K. P. McKenna, *J. Chem. Theory Comput.*, 2018, **14**, 3740.

Received: 28th November 2022; Com. 22/7052